Asian Journal of Chemistry; Vol. 33, No. 7 (2021), 1541-1550

ASIAN JOURNAL OF CHEMISTRY

https://doi.org/10.14233/ajchem.2021.23197

New Carbazole-Based Organic Dyes with Various Acceptors for Dye-Sensitized Solar Cells: Synthesis, Characterization, DSSCs Fabrications and DFT Study

T. SARAVANA KUMARAN[1,*], A. PRAKASAM[1], P. VENNILA[2], S. PARVEEN BANU[3] and G. VENKATESH[4]

[1]Department of Physics, Thiruvalluvar Government Arts College, Rasipuram-637408, India
[2]Department of Chemistry, Thiruvalluvar Government Arts College, Rasipuram-637408, India
[3]Department of Physics, Sri Kailash Women's College, Salem-636112, India
[4]Department of Chemistry, Muthayammal Memorial College of Arts & Science, Rasipuram-637408, India

*Corresponding author: E-mail: vsasrvn@gmail.com

Received: 7 March 2021; *Accepted*: 22 April 2021; *Published online*: 26 June 2021; AJC-20395

The molecular configuration, synthesis and characterization of (*E*)-3-(6-bromo-9-phenyl-9*H*-carbazol-3-yl)acrylic acid (BPA), (*E*)-3-(6-bromo-9-phenyl-9*H*-carbazol-3-yl)-2-cyanoacrylic acid (BPCA) and (*E*)-*N*′-((6-bromo-9-phenyl-9*H*-carbazol-3-yl)methylene)-2-cyanoacetohydrazide (BPCH) configured D-π-A sensitizers and the sensitizers are used in DSSCs. Dye molecules are described by FT-IR, NMR and UV-Vis analysis. The study shows that the non-planar structure of BPA, BPCA and BPCH can effectively slow down the aggregation and conjugation of the dye. Computed vibrational modes are compared with observed bands. The Frontier molecular orbital (FMO) and molecular electrostatic potential (MEP) have also been calculated using DFT-B3LYP/6-311++G(d,p) basis set. Physical-chemical parameters have also been analyzed using density functional theory. The most excellent DSSC performance in photovoltaic characterization is demonstrated by the dye molecules.

Keywords: Carbazole, Dye-sensitized solar cells, Density Functional theory, Molecular electrostatic potential, Frontier molecular orbital.

INTRODUCTION

One of the most powerful inventions is a photovoltaic device that directly converts sunlight into electricity [1-3]. Dye-sensitized solar cells (DSSCs) are at the threshold of commercial exploitation of innovation among numerous categories of photovoltaic technology available in the future generation of solar cells. In the light of photovoltaic technologies, DSSCs have unique basic construction and manufacturing processes beyond their efficiency, which lead to the growth of their use as a power supply [3-6]. The advantages of the DSSC include, but are not restricted to the cost effective of the manufacturing process, excellent performance under low light conditions and opportunities for molecular design. The sensitizer has been one of the major ingredients for achieving high efficiency and longevity of the system [7].

Organic dyes have a major role to play in electron injection and light harvesting to achieve high performance. Among the different synthetic dye carbazole dependent sensitizers are possible candidates holding a high position attributable with electron-rich nitrogen and sulphur atoms making the electron donor stronger than other *N*-heterocyclic such as triphenylamine and carbazole [8,9]. Carbazole and its derivatives are widely used donors for the sensitization of dyes due to their strong hole transport capabilities and large band gap [10]. Many sensitizing carbazole dyes with excellent photovoltaic efficiency have been documented. A further approach for molecular engineering of sensitizing dyes is the incorporation of an auxiliary acceptor. The implementation of an additional acceptor has shown that it can help shift the charge from the donor to the acceptor and expand the conjugation system, thereby enhancing the visible response of the region [10-12]. The molecular structure of the dye is among the most significant influences in regulating the efficacy of the DSSCs. It is highly responsible for the absorption of sun energy and the transition of energy between both the semiconductor and the electrolyte. The stimulated electron is inserted into the semiconductor electrode whereas the oxidized dye is preserved *via* an electrolyte that

in turning, absorbs electrons through the counter electrode in order to accomplish the circuit [9-12].

The configuration of organic dyes as in shape of a conjugated donor-linker-acceptor (D-π-A) does have a beneficial impact on the reliability and efficiency of the DSSCs. Recently, acrylic cyanide and cyanide classes are often used for an electrode bound acceptor and anchor. Consequently, three novel carbazoles based on dye molecules were synthesized using various donor units. In addition, these dye molecules are described in the FT-IR, UV-Vis and NMR studies. In addition, photophysical, quantum chemical, molecular electrostatic potential and photovoltaic properties have also been studied with the help of density functional theory.

EXPERIMENTAL

All the chemicals have been procured through Sigma-Aldrich and Spectrochem and used without further purification. Further, molecular structural analysis are performed by using ^{1}H &^{13}C NMR chemical shifts were recorded in DMSO-d_6 solvent on a 400 MHz Bruker Avance spectrophotometer and Ultraviolet-Visible absorption spectra was measured at room temperature utilizing Analytik Jena SPECORD S 600 spectrometer. The FT-IR spectrum was recorded on the Jasco FT-IR 4700 A spectrophotometer.

Synthesis of dye compounds: Phosphorus oxychloride (9.18 mL) was added dropwise to distilled DMF (10 mL) and the mixture of 9-phenyl-9*H*-carbazole (11.03 g, 45.4 mmol) and DMF (25 mL) were also added dropwise to phosphorus oxychloride/DMF mixture at room temperature. The mixture constant stirring continuously for 2 h at 80 ºC and left at room temperature, after pouring ice water and then neutralized with NaOH up to 7-8 pH, after slowly forming brown precipitate. It has been filtered using methanol and purified by column chromatography (ethyl acetate/hexane). In addition, 9-phenyl-9*H*-carbazole-2-carbaldehyde (11.53 g) and ethanol (125 mL) were incorporated into a 250 mL flask and then 10 g BrCl was progressively added to the mixture at 75 ºC (0.5 drop/s) until the reaction was completed. A brown solid (6-bromo-9-phenyl-9*H*-carbazole-2-carbaldyde) formed and recrystallized by anhydrous ethanol.

The dye compounds *viz*. (*E*)-3-(6-bromo-9-phenyl-9*H*-carbazol-3-yl)acrylic acid (BPA), (*E*)-3-(6-bromo-9-phenyl-9*H*-carbazol-3-yl)-2-cyanoacrylic acid (BPCA) and (*E*)-*N*′-((6-bromo-9-phenyl-9*H*-carbazol-3-yl)methylene)-2-cyanoacetohydrazide (BPCH) were synthesized. In brief, a solution of acetonitrile (20 mL) and 6-bromo-9-phenyl-9*H*-carbazole-2-carbaldyde (19.5 mmol) was individually added to 42 mmol propanedioic acid, cyanoacetic acid and 2-cyanoacetohydrazide along with 9 mmol of piperidine after continuously stirred at 90 ºC for around 2 h. The organic layer produced after the completion of the reaction has been filtered and extracted column chromatography in the chloroform/methanol mixture through silica gel (**Scheme-I**).

Dye compound (BPA): m.p.131-134 ºC, *m.w.*: 392.25, m.f.: $C_{21}H_{14}NO_2Br$. Mass *m/z*: 391.02 (100.0%), 393.02 (97.4%), 392.02 (23.1%), 394.02 (22.5%), 393.03 (2.9%), 395.03 (2.5%). Elemental analysis (%): C, 64.30; H, 3.60; Br, 21.05; N, 3.54; O, 8.21. ^{1}H NMR (DMSO-d_6, 400 MHz) δ ppm: 9.18 (1H, d, Ar-H), 8.17 (1H, d, Ar-H), 8.12 (1H, d, Ar-H), 7.96 (1H, d, Ar-H), 7.55 (1H, d, Ar-H), 7.46 (1H, d, Ar-H), 7.44 (1H, d, Ar-H), 7.23 (1H, d, Ar-H), 6.99 (1H, t, Ar-H), 6.26 (1H, d, Ar-H), 3.02 (2H, s). ^{13}C NMR (125 MHz DMSO-d_6) δ ppm: 161.62, 129.42, 126.18, 121.54, 121.11, 113.48, 112.29, 112.15, 111.06, 105.69, 102.25, 101.26, 100.64, 99.88, 98.78, 97.85, 95.91, 95.61, 93.75, 66.34, 55.61.

Dye compound (BPCA): m.p.139-142 ºC, *m.w.*: 417.25, *m.f.*: $C_{22}H_{13}N_2O_2Br$. Mass *m/z*: 416.02 (100.0%), 418.01 (97.3%), 417.02 (24.0%), 419.02 (23.5%), 418.02 (3.3%), 420.02 (3.1%). Elemental analysis (%): C, 63.29; H, 3.21; Br, 19.22; N, 6.69; O, 7.71. ^{1}H NMR (DMSO-d_6, 400 MHz) δ ppm: 9.32 (1H, d, Ar-H), 7.98 (1H, d, Ar-H), 7.84 (1H, d, Ar-H), 7.24 (1H, d, Ar-H), 7.11 (1H, d, Ar-H), 7.02 (1H, d, Ar-H), 6.98 (1H, d, Ar-H), 6.91 (1H, d, Ar-H), 6.88 (1H, t, Ar-H), 6.65 (1H, d, Ar-H), 6.29 (1H, d, Ar-H), 2.84 (2H, s). ^{13}C NMR (125 MHz DMSO-d_6) δ ppm: 165.38, 139.77, 129.34, 126.41, 121.98, 116.48, 115.46, 113.34, 113.09, 113.05, 112.95, 112.31, 111.12, 107.77, 106.31, 102.94, 102.16, 102.08, 101.25, 88.25, 45.13.

Dye compound (BPCH): m.p.: 158-164 ºC, *m.w.*: 431.28, m.f.: $C_{22}H_{15}N_4OBr$. Mass: *m/z* 430.04 (100.0%), 432.04 (97.6%), 433.04 (24.6%), 431.05 (24.0%), 432.05 (3.0%), 434.05 (2.9%), 431.04 (1.5%). Elemental analysis (%): C, 61.32; H, 3.49; Br, 18.61; N, 12.99; O, 68. ^{1}H NMR (DMSO-d_6, 400 MHz), δ ppm: 8.64 (1H, d, Ar-H), 7.92 (1H, d, Ar-H), 7.86 (1H, d, Ar-H), 7.54 (1H, d, Ar-H), 7.16 (1H, d, Ar-H), 6.98 (1H, d, Ar-H), 6.92 (1H, d, Ar-H), 6.88 (1H, d, Ar-H), 6.75 (1H, t, Ar-H), 6.51 (1H, d, Ar-H), 6.24 (1H, s), 3.03 (2H, s), 2.82 (2H, s), 2.76 (2H, s). ^{13}C NMR (125 MHz DMSO-d_6) δ ppm: 168.19, 124.22, 122.24, 121.41, 116.82, 114.09, 110.82, 110.76, 110.21, 109.18, 108.85, 108.24, 106.84, 104.42, 104.26, 103.85, 102.56, 98.21, 91.02, 32.28.

Computational details

Geometrical optimizations of the title molecules were performed using DFT/B3LYP functional and 6-311++G(d,p) level in the gas phase [13]. Electronic absorption spectra for BPA, BPCA and BPCH molecules have been determined utilized TD-DFT-B3LYP (TD-B3LYP). The TD-DFT and DFT calculations have been carried out using Gaussian 09W package. The molecular orbital energies of HOMO and LUMO are related directly to the ioni-zation potential (IP) and the electron affinity (EA), respectively within the Koopmans theorem [14-19]:

$$\text{Ionization potential} = -E_{HOMO} \quad (1)$$

$$\text{Electron affinity} = -E_{LUMO} \quad (2)$$

Electronegativity (χ) could be described as the electron donation ability of the molecule and can also be established as the negative of the chemical potential (μ):

$$\mu = -\chi = \left\{\frac{E_{LUMO} + E_{HOMO}}{2}\right\} \quad (3)$$

Chemical hardness (η), electrophilicity index (ω) and nucleophilicity (ε) could be calculated by

$$\eta = \left\{\frac{E_{LUMO} - E_{HOMO}}{2}\right\} \quad (4)$$

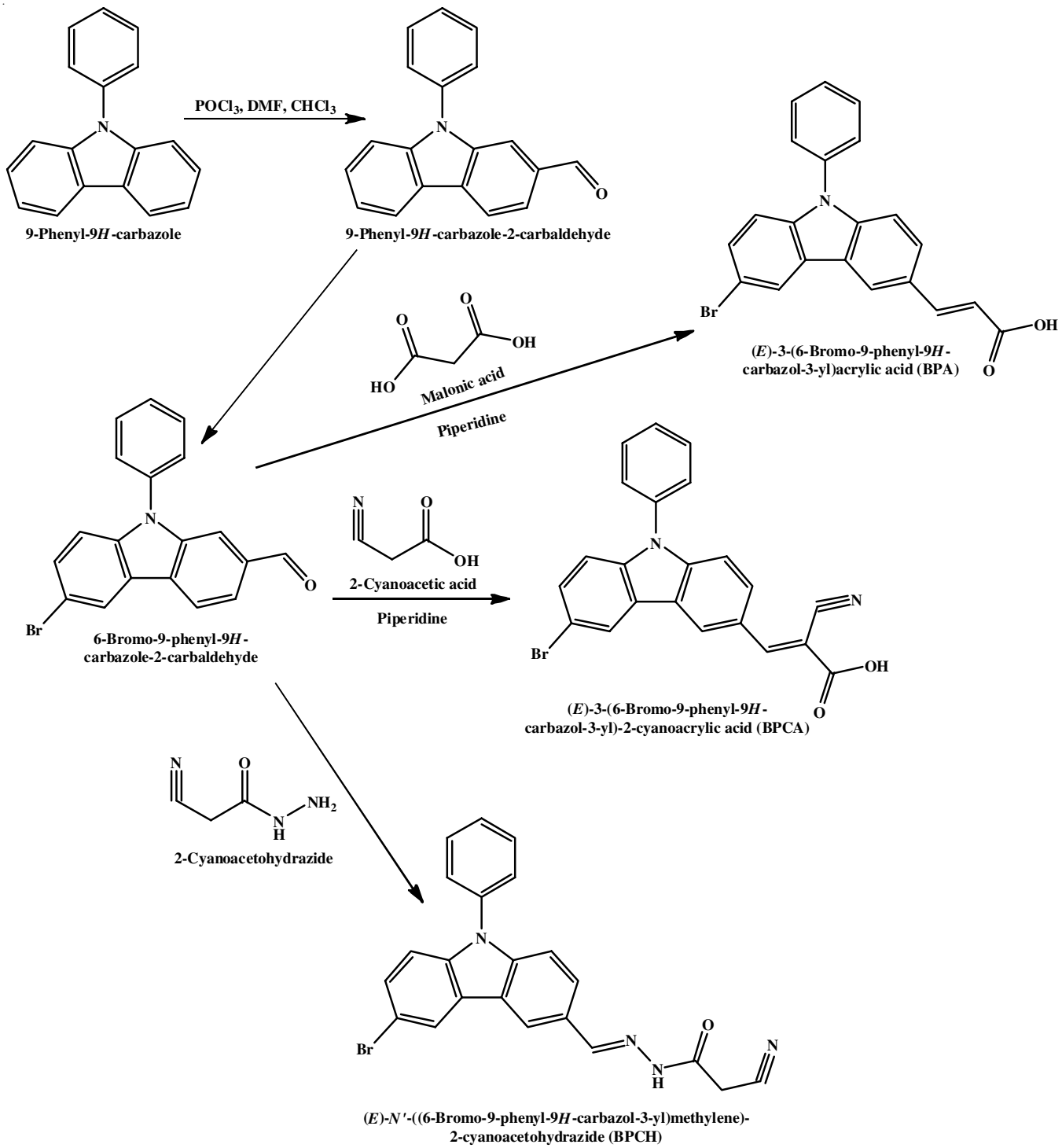

Scheme-I: Synthetic procedure of the target organic dyes

$$\sigma = \frac{1}{\eta} \quad (5)$$

$$\omega = \frac{\mu^2}{2\eta} \quad (6)$$

$$\varepsilon = \frac{1}{\omega} \quad (7)$$

Similarly, the electron-accepting capacity (ω^+) can be calculated as

$$\omega^+ = \frac{(1+3EA)^2}{16(IP-EA)} \quad (8)$$

Approximately the LHE was determined from the oscillator strength (f) as shown in eqn. 9 and ΔG^{inject} have been determined using eqn. 10:

$$LHE = 1–10^{-f} \quad (9)$$

$$\Delta G^{inject} = E^{OX}_{dye*} - E^{TiO_2}_{CB} \quad (10)$$

where, E^{OX}_{dye*} → unrelaxed excited state oxidation potential and $E^{TiO_2}_{CB}$ → charge of the conduction band minimum (CBM) of the semiconductor. E^{OX}_{dye*} was calculated by using eqn. 11:

$$E^{OX}_{dye*} = E^{dye}_{OX} - \Delta Es_{ICT} \quad (11)$$

where, ΔEs_{ICT} → vertical excitation energy and E^{dye}_{OX} → negative charge of the highest occupied molecular orbital [20-23].

V_{oc} was calculated from the energy difference between the dye's lowest unoccupied molecular orbital (LUMO) as a donor and the conduction band minimum (CB) as an acceptor (eqn. 12 in eV).

$$V_{oc} = E_{LUMO} - E_{CB} \quad (12)$$

RESULTS AND DISCUSSION

Molecular structural analysis: The optimized studied dye molecules are shown in Fig. 1. The dyes BPA, BPCA and BPCH contain bromo phenyl carbazole as the oxidizing donor species and acrylic acid, cyanoacrylic acid and cyanoacetohydrazide acid as the accepter reduction species, connected through π-bridge of carbon atom. The π-bridge carbon atom acts as a charging channel for the movement of electrons from the donor to the acceptor species, which is eventually transferred to the semiconductor. The C2=C3 for BPA and BPCA bond length was found 1.32 Å and 1.33 Å, respectively which indicate that the double bond character occurs between C-C atoms [24,25]. Further, C8=N5 bond length is 1.29 Å for BPCH indicates double character. C7=N7 bond length was 1.18 (PBCA), 1.16 (BPCH) Å showed that triple bond character. The calculated C-Br bond length is 1.95 Å (BPA), 1.92 Å (BPCA) and 1.94 Å (BPCH). In addition, an entire species contains coplanar atoms, except for the *N*-benzyl phenyl ring, which means that electron delocalization occurs within the molecule. In addition, the bond length and bond angle values of the synthesized compounds have also shown that N and aromatic C atoms in the molecule have a sp^2 hybrid structure. The calculated bond angle of C7-N6-C18 (108.45°), C18-N6-C19 (125.63º), C10-C3-C2 (127.36º), C3-C2-C1 (123.69º), O4-C1-O5 (120.91°) for BPA and C6-C2-C3 (125.05º), C9-N8-C20 (107.02º), C9-N8-C21 (126.61º), C10-C17-C18 (120.96º), C2-C3-C12 (132.03º), O5-C1-O4 (122.23º), N7-C6-C2 (179.11º) for BPCA and C10-N9-C21 (108.78º), C10-N9-C22 (125.68º), C17-C18-C19 (121.33º), N5-C8-C13 (130.25º), C1-N4-N5 (120.02º), C6-C2-C1 (111.22º), C2-C1-C3 (124.95º) for BPCH indicates intramolecular interaction between D to A. Further, the calculated dihedral angle of O4-C1-C2-C3 (-179.96º), O5-C1-C2-C3 (0.02º), C1-C2-C3-C10 (-179.45º) for BPA and C1-C2-C3-C12 (180.0º), O5-C1-C2-C3 (179.24º) for BPCA and N4-N5-C8-C13 (-3.53º), N7-C6-C2-C1 (179.19º), O3-C1-N4-N5 (174.91º), N5-C8-C13-C14 (143.78º) indicates slightly coplanar of the carbazole ring.

Absorption properties: The most important necessities that a dye molecule could be address their absorption in the visible region [2]. The experimental UV-Vis absorption spectra of BPA, BPCA and BPCH molecules are obtained using DMSO solution and shown in Fig. 2. The UV-Vis spectra of BPA, BPCA and BPCH display two prominent 280-360 nm and 360-650 nm peaks, respectively. The prior is assigned to a localized π–π* aromatic transformation while the latter is of a charge-transfer character. The absorption maxima (λ_{max}) of BPA, BPCA and BPCH are allocated at 494, 468 and 505 nm, respectively. Compared to PBA and BPCA, BPCH increased the rate of electron delocalization over the entire molecule; however its overall absorption peak appeared red shifted. The electronic absorption peaks of the dyes were computed using TD-DFT-B3LYP function/6-311G++(d,p) in the DMSO solvent phase and shown in Fig. 3. The calculated absorption wavelengths of the title dyes were calculated at 478.11, 351.54,

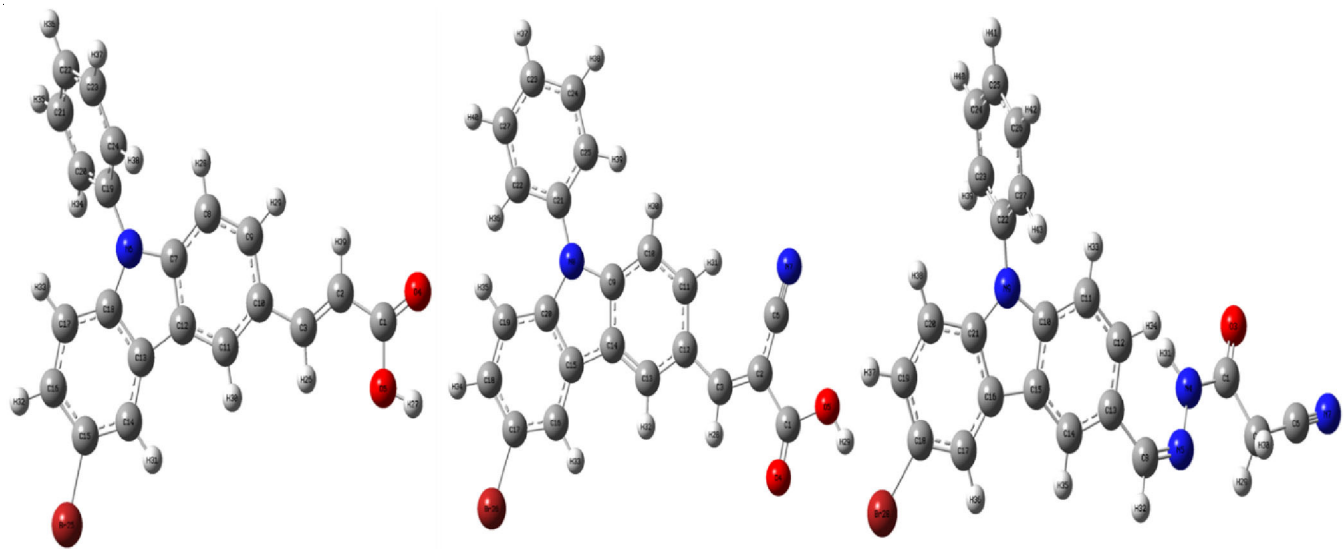

Fig. 1. Optimized structure of studied compounds

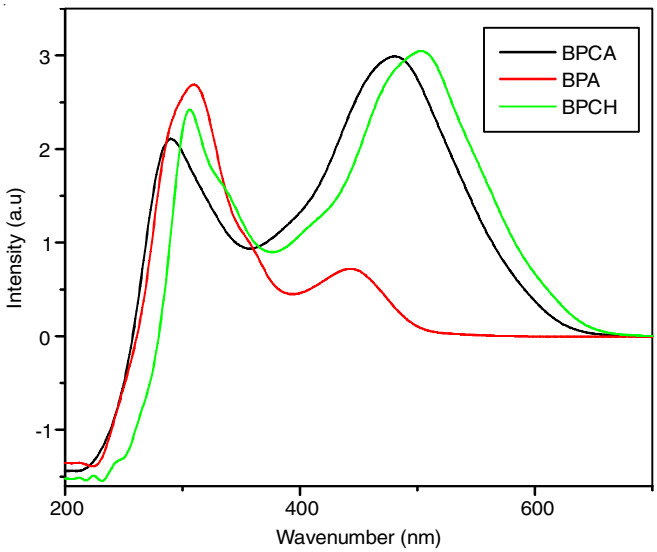

Fig. 2. UV-vis absorption spectra of BPA, BPCA and BPCH

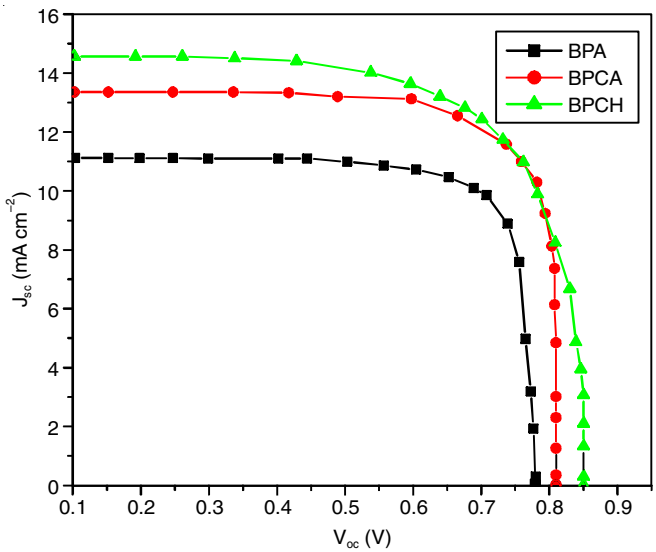

Fig. 3. J-V curve of device sensitized with studied compounds

311.46 nm (BPA), 466.24.24, 348.64.64, 316.28 nm (BPCA) and 481.36, 364.52, 306.91 nm (BPCH), respectively and shown in Table-1.

Photosensitizations and electronic properties: Previously, they measured the amount of dye loaded on the surface of TiO_2 by desorbing the adsorbed sensitizer and the amount obtained is shown in Table-2. The photovoltaic output of the system title dye molecules is described using 100 mW cm^{-2} simulated AM 1.5G sun energy with cover and associated current density-voltage (J-V) plot [1-3]. Adsorbed concentrations of BPA, BPCA and BPCH are found to be 5.05×10^{-7}, 5.15×10^{-7} and 4.68×10^{-7} mol cm^{-2}, respectively. The lower volume of BPCA and BPCH dye loading relative to BPA may be due to the increased molecular size of the prior dyes. Fig. 4 reveals that both BPCA and BPCH sensitizers have a high short-circuit current (J_{sc}) of ~13.51 and 14.72 mA/cm^{-2}, while in the case of BPA sensitizers the values were lower at ~11.18 mA/cm^{-2}. Open-circuit voltage (V_{oc}) and BPA, BPCA and BPCH filling factors vary from 0.78 to 0.85 V. In addition, ΔG^{inject}, light harvesting

TABLE-1
PHOTO PHYSICAL PROPERTIES OF STUDIED COMPOUNDS

Parameters	BPA	BPCA	BPCH
f	0.2102	0.4281	0.0336
	0.2245	0.1261	0.3503
	0.0801	0.1677	0.1303
LHE (1-10^{-f})	0.3836	0.6268	0.0744
	0.4036	0.2521	0.5536
	0.1682	0.3203	0.2592
λ_{max} (nm)	478.11	466.24	481.36
	351.54	348.64	364.52
	311.46	316.28	306.91
E(0,0) (eV)	3.75	3.08	4.00
	3.80	3.50	4.04
	4.04	3.91	4.46
E_{HOMO} (eV)	-6.07	-6.03	-7.41
E_{LUMO} (eV)	-1.93	-2.64	-0.57
Edye (eV)	6.07	6.03	7.41
E*dye (eV)	2.32	2.95	2.41
	2.23	2.52	2.37
	3.37	2.11	1.99
V_{oc}	-5.93	-6.64	-4.57
ECB (eV)	-4.0	-4.0	-4.0
ΔG^{inject} (Kcal/mol)	-38.77	-24.23	-36.61
	-39.96	-34.07	-37.53
	-45.50	-43.48	-46.46

TABLE-2
PHOTOVOLTAIC MEASUREMENT DATA OF FABRICATED DSSCs

Dye	J_{sc} (mA cm^{-2})	V_{oc} (V)	FF	η (%)	Adsorbed amount of dye (mol cm^{-2})
BPA	11.18	0.78	0.69	6.72	5.05×10^{-7}
BPCA	13.57	0.81	0.71	7.46	5.15×10^{-7}
BPCH	14.72	0.85	0.68	8.12	4.68×10^{-7}

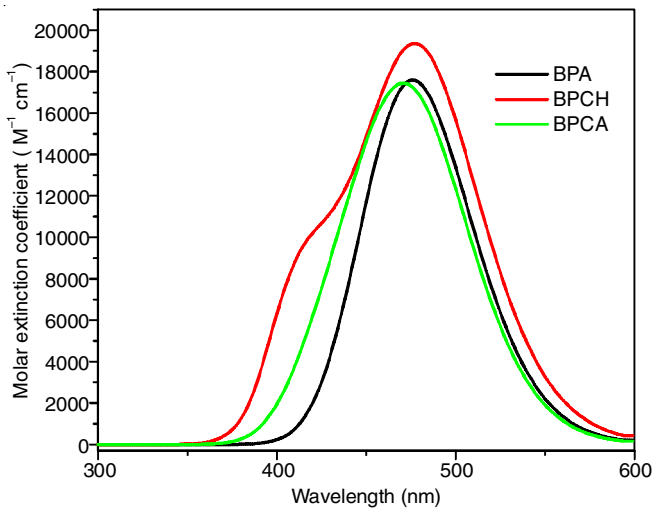

Fig. 4. Simulated absorption spectrum of BPA, BPCA and BPCH

energy (LHE), oscillator strength (f) and vertical excitation energy of the title dye molecules are theoretically calculated and shown in Table-1. The studies strongly support the use of title compounds for the development of DSSCs.

Frontier molecular orbital (FMO) approach: FMO of HOMO and LUMO is related to the ionization potential and

electron affinity and predicts the high reactive position in the ambient electron systems and also describes various forms of reactions in the conjugate system [3,26]. Fig. 5 has shown that the HOMO orbital is located on the phenyl carbazole ring; the LUMO orbital is located on the acceptor group's acrylic acid, cyanoacrylic acid and cyanoacetohydrazide. The energy gap is an essential factor for deciding the properties of molecular electrical transport. The band gap energy of BPA, BPCA and BPCH as 4.13, 3.38 and 6.83 eV, respectively and also clear that these dye molecules are highly suitable for DSSCs performances. Important quantum chemical parameters of chemical hardness, softness, electrophilicity index and nucleophilicity and electron acceptance of power are also evaluated using the B3LYP function/6-311++G(d,p) basic set in the gas phase as listed in Table-3. Hardness and softness are related to the polarization and stability of the molecules. The electron-accepting efficiency is related to the interaction between the acceptor and the donor unit within the molecule. The results indicate that BPCH is considerably better than BPA and BPCA.

Molecular electrostatic potential (MEP): The MEP is used to determine the relative reactivity of nucleophilic and electrophilic attacks in the entire system [27-29]. The MEP surface description of the title molecules is calculated by DFT analysis utilizing the optimized B3LYP function 6-311G++ (d,p) basis set. MEP surface of title molecules is given in Fig. 6, which indicates that negative potential areas are positioned above the electronegative atoms oxygen, bromine and nitrogen and also the positive potential sections are located aromatic ring and protons. As a consequence, the negative potential donor and positive potential receptor reactive sites are quite responsive to the attraction of its nucleophilic and electrophilic molecular environment. Finally, the results concluded that BPA, BPCA and BPCH are totally beneficial for DSSC applications.

Analysis of vibrational spectra: The observed and computed vibration frequency of BPA, BPCA and BPCH with intensity values can be seen in Figs. 7 and 8. Further, the wavenumbers are scaled with 0.967 and compared with experimental frequencies given in Table-4. Comprehensive scaled and observed bands correlated with their assignments together with total energy distributions for BPA, BPCA and BPCH are shown in Table-4. N-Ph stretching frequencies are complicated, since it is difficult to differentiate against other aromatic ring vibrations. For the substituted aromatic rings, the N-Ph stretching frequency observed in 1400-1200 cm^{-1} range [30-32]. The experimental N-Ph stretching bands assigned at 1292, 1145 cm^{-1} (BPA), 1133 cm^{-1} (BPCA) and 1614, 1458 cm^{-1} (BPCH) agreed with the sealed modes.

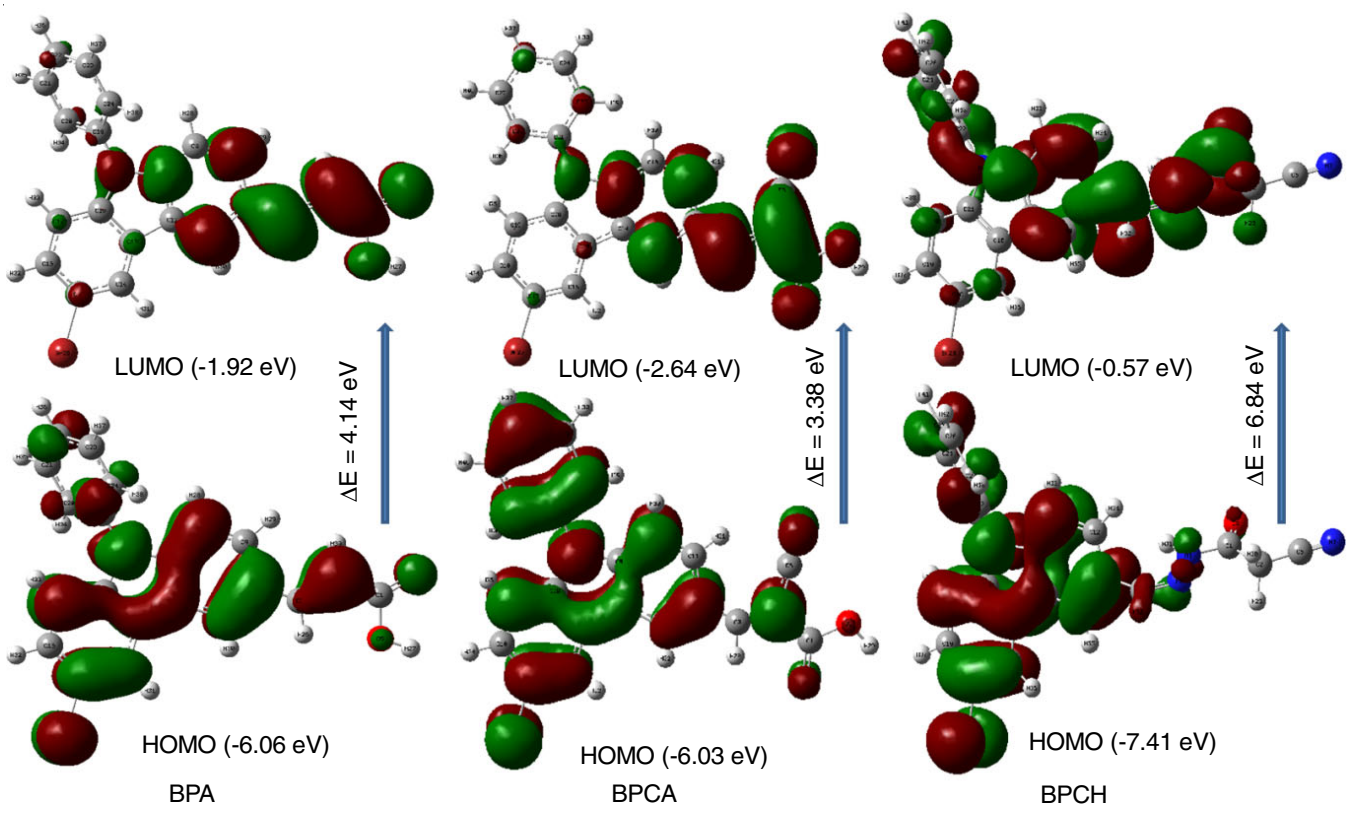

Fig. 5. FMO energy levels of BPA, BPCA and BPCH

TABLE-3
QUANTUM CHEMICAL PARAMETER OF STUDIED COMPOUNDS

HOMO	LUMO	IP	EA	ΔE	χ	μ	η	σ	ω	ε	ω^+
-5.75	-1.84	5.75	1.84	3.91	-3.79	-3.79	1.96	0.51	3.68	0.27	0.68
-6.03	-2.64	6.03	2.64	3.39	-4.33	-4.33	1.70	0.59	5.53	0.18	1.46
-7.41	-0.58	7.41	0.58	6.83	-3.99	-3.99	3.42	0.29	2.33	0.43	0.07

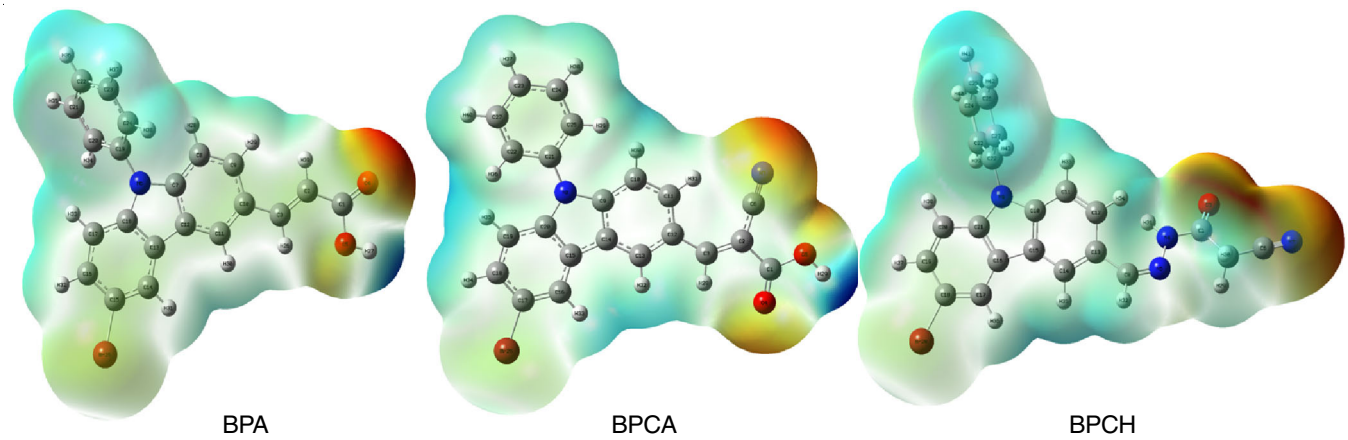

Fig. 6. MEP image of BPA, BPCA and BPCH

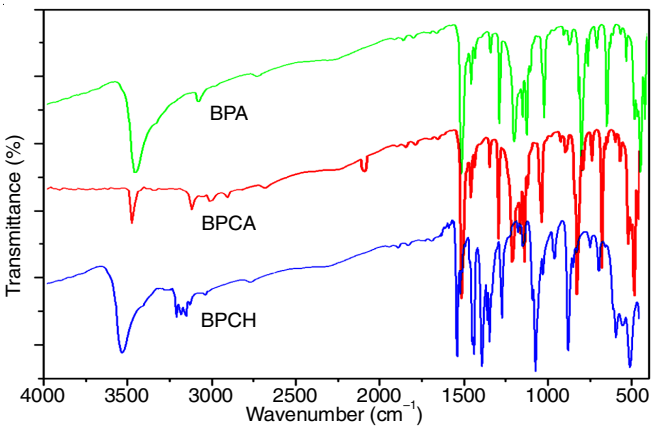

Fig. 7. FT-IR spectrum of studied compounds

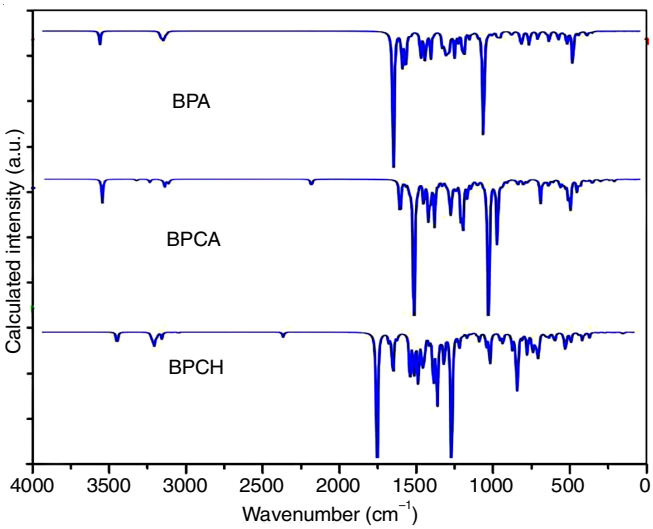

Fig. 8. Stimulated vibrational spectra of studied compounds

The N-H stretching bands generally occur at 3500-3400 cm^{-1} ranges. The observed N-H stretching modes of BPCH occur at 3558 (3568 calcd.) cm^{-1}. In addition, observed stretching bands of C-N appeared at 2192 cm^{-1} (BPCA), 2264 cm^{-1} (BPCH) and are agreed with computed bands (2199, 2279 cm^{-1}). C-H stretching vibration is usually observed at 2900-3300 cm^{-1} [32]. In present study, C-H stretching vibrations observed at 3133, 3112, 3098, 3086 cm^{-1} (BPA), 3142, 3135, 3122, 3098, 3076 cm^{-1} (BPCA) and 3155, 3146, 3141, 3128 cm^{-1} (BPCH). The in-plane bending vibrations of C-H originate in the range 1000-1300 cm^{-1}. In present work, the experimental C-H in-plane bending bands originated at 1341, 1310, 1188, 1084, 1028 cm^{-1} (BPA), 1325, 1322, 1145, 1112, 1079 cm^{-1} (BPCA) and 1341, 1259, 1156, 1038 cm^{-1} (BPCH) and are well correlated with sealed vibration modes. Out-of-plane bending vibrations of C-H are closely coupled vibrations and usually occur within the range 1000-700 cm^{-1} [29]. The observed FT-IR vibrations frequency appeared at 934, 910, 880, 775, 710 cm^{-1} (BPA), 940, 892, 871, 776, 758, 742, 713 cm^{-1} (BPCA) and 945, 928, 868, 839, 754 cm^{-1} (BPCH) are correlated with the computed modes. Commonly, aromatic stretching modes occur in the range of 1650-1400 cm^{-1}. In present analysis, CC vibrational stretching frequencies appear at 1668, 1620, 1600, 1575, 1488 cm^{-1} for BPCA and 1612, 1598, 1519, 1472, 1325, cm^{-1} for BPCA and 1581, 1492, 1368, 1341 cm^{-1} for BPCH, which are correlated well with calculated modes. At 1632 cm^{-1} for BPCA, 1648 cm^{-1} for BPCH, C-O stretching vibrations in FT-IR were observed. At 3521 cm^{-1} in FT-IR, O-H stretching vibrational frequencies of BPA is assigned, while 3524 cm^{-1} for BPCA. Intense absor-ption by the C-Br stretching vibration is found, which affects the neighbor's superior effect by the neighboring atoms or group (narrower halide atom). Generally, C-Br stretching vibrations occur in regions of 850-480 cm^{-1}. At 631, 498 and 628 cm^{-1} in FT-IR, the C-Br stretching vibration bands of BPA, BPCA and BPCH are assigned and correlate well to the calculated bands. The first scrutiny's performance inspired us to undertake a detailed assignment of the experimentally observed bands.

Conclusion

Three novel organic dyes based on carbazole, (*E*)-3-(6-bromo-9-phenyl-9*H*-carbazol-3-yl)acrylic acid (BPA), (*E*)-3-(6-bromo-9-phenyl-9*H*-carbazol-3-yl)-2-cyanoacrylic acid (BPCA) and (*E*)-*N*′-((6-bromo-9-phenyl-9*H*-carbazol-3-yl)-methylene)-2-cyanoacetohydrazide (BPCH) were efficiently designed, synthesized and well-characterized. From their photo-physical and physico-chemical perspective, this indicates that these dye molecules have all the necessary conditions to act

TABLE-4
DETAILED VIBRATIONAL FREQUENCIES OF STUDIED COMPOUNDS

Experimental			BPA		BPCA		BPCH		PET		
BPA	BPCA	BPCH	Cal. IR	Intensity	Cal. IR	Intensity	Cal. IR	Intensity	BPA	BPCA	BPCH
3521	3524	3558	3512	7.70	3514	12.47	3568	7.82	νOH(100)	νOH(100)	νNH(100)
–	–	3155	3138	0.72	3300	0.63	3154	0.99	νCH(84)	νCH(68)	νCH(63)
3133	–	–	3134	1.83	3297	0.47	3146	1.85	νCH(84)	νCH(88)	νCH(65)
–	3142	3146	3130	0.58	3218	1.27	3144	0.50	νCH(92)	νCH(96)	νCH(68)
–	–	–	3128	0.61	3215	0.63	3143	0.47	νCH(89)	νCH(87)	νCH(84)
–	–	3141	3124	0.46	3151	0.40	3139	2.08	νCH(86)	νCH(94)	νCH(85)
–	3135	–	3122	0.82	3132	0.04	3137	0.69	νCH(80)	νCH(96)	νCH(66)
–	–	3128	3120	1.10	3131	0.27	3131	5.59	νCH(58)	νCH(98)	νCH(66)
3112	3122	–	3114	3.97	3125	4.24	3124	1.15	νCH(93)	νCH(97)	νCH(92)
–	–	–	3109	1.08	3103	2.19	3121	0.43	νCH(89)	νCH(99)	νCH(84)
–	3098	3114	3103	0.75	3097	0.56	3114	1.42	νCH(87)	νCH(99)	νCH(98)
3098	–	–	3096	1.10	3096	0.44	3111	0.39	νCH(90)	νCH(97)	νCH(99)
–	3076	3088	3095	0.31	3074	0.05	3085	3.59	νCH(86)	νCH(99)	νCH(99)
3086	2192	3026	3088	0.08	2199	4.47	3025	0.15	νCH(91)	νNC(89)	νCH(55)
1668	–	2996	1677	100.00	1663	24.87	2979	0.53	νCC(62)	νCC(12)	νCH(94)
–	1632	2264	1628	3.73	1629	2.37	2279	2.88	νCC(11)	νOC(75)	νNC(88)
1620	1612	–	1621	17.52	1607	5.11	1724	100.00	νCC(70)	νCC(10)	νCC(12)
–	–	1648	1603	8.87	1601	0.18	1650	5.05	νCC(49)	νCC(25)	νOC(79)
1600	1598	–	1599	16.72	1595	2.58	1632	2.16	νCC(58)	νCC(58)	νCC(10)
–	–	–	1589	0.98	1577	100.00	1625	3.41	νCC(14)	νCC(40)	νCC(14)
1575	–	–	1573	1.37	1574	6.40	1621	23.65	νCC(62)	νCC(46)	νCC(17)
–	–	1614	1564	1.48	1554	5.01	1610	1.17	νCC(55)	νCC(38)	νNC(61)
–	1519	–	1506	16.86	1516	16.15	1595	3.12	νCC(52)	νCC(50)	νCC(20)
1488	–	1581	1482	14.31	1486	24.14	1582	0.22	νCC(50)	νCC(21)	νCC(26)
–	1472	–	1471	6.94	1473	8.81	1515	32.70	νCC(12)	νCC(19)	νCC(21)
–	–	1492	1463	0.40	1463	0.85	1491	20.30	σHCC(59)	σHCC(17)	νCC(25)
–	1442	–	1443	16.23	1448	25.53	1485	7.72	σHCC(21)	δCCC(44)	νCC(16)
–	–	–	1424	1.58	1426	2.31	1468	1.07	σHCC(15)	σHCC(19)	νCCC(12)
–	–	1458	1371	7.84	1401	3.36	1462	31.31	νCC(12)	σHCC(11)	νNC(12)
–	–		1360	5.35	1376	3.47	1443	7.40	σHCC(19)	σHCC(28)	σHCC(12)
–	–	–	1351	9.96	1359	7.01	1431	19.47	γCCN(10)	σHCC(21)	σHCC(15)
1341	–	–	1345	2.28	1348	14.14	1422	6.80	σHCC(55)	νCC(27)	σHCC(18)
–	–	–	1338	9.87	1343	6.51	1396	4.60	νCC(22)	νCC(14)	σHCC(11)
–	1325	1388	1328	10.76	1329	3.02	1385	1.31	σHCC(12)	σHCC(41)	νCC(22)
–	1322	–	1315	1.01	1314	6.37	1370	14.27	δCCC(48)	σHCC(52)	σHCC(11)
1310	–	1368	1311	0.81	1287	14.72	1364	17.15	σHCC(56)	νCC(52)	νCC(10)
1292	–	–	1294	14.27	1282	10.74	1356	0.61	νNC(56)	νCC(25)	νCC(10)
–	1274	1341	1272	5.39	1271	23.26	1343	44.24	νCC(42)	νOC(49)	σHCC(28)
–	–	–	1245	12.10	1246	10.30	1331	3.66	σHCC(17)	νCC(18)	δCCC(15)
–	1228	1312	1234	11.65	1222	5.17	1314	2.82	νCC(13)	σHOC(17)	σHNN(14)
–	–	–	1202	3.97	1210	0.32	1299	20.07	σHCC(11)	CCC(10)	νCC(18)
1188	–	1259	1192	0.08	1189	0.76	1257	19.38	σHCC(53)	νCC(49)	σHCC(78)
–	–	–	1184	0.01	1182	3.19	1253	51.71	σHCC(48)	νCC(19)	νCC(13)
–	1145	1250	1183	1.23	1147	1.97	1249	22.44	νCC(17)	σHCC(18)	σHCN(34)
1145	1133	–	1147	2.39	1131	2.23	1207	0.00	νNC(14)	νNC(24)	νNC(15)
–	–	1205	1125	3.39	1116	63.86	1204	9.15	νNC(31)	σHCC(14)	νNC(14)
–	1112	–	1113	73.98	1110	36.68	1190	0.82	νCC(13)	σHCC(36)	σHCC(11)
1084	1079	1185	1086	0.67	1078	1.65	1185	0.01	σHCC(83)	σHCC(58)	δCCC(16)
–	–	–	1059	2.33	1060	40.26	1180	1.27	δCCC(20)	σHCC(31)	σHCC(21)
1028	–	1156	1030	0.62	1040	0.91	1154	2.87	σHOC(47)	δCCC(12)	σHCC(31)
–	1026	–	1026	3.50	1028	4.00	1130	0.99	δCCC(42)	νNC(21)	σHCC(21)
–	–	1092	1011	4.62	1003	0.09	1091	1.43	δCCC(25)	δCCC(12)	νNC(10)
–	–	–	1005	0.25	999	1.50	1076	5.00	δCCC(23)	δCCC(38)	τHCCN(10)
–	–	1038	1002	0.00	992	0.02	1037	1.17	δCCC(44)	δCCC(15)	σHCC(37)
975	962	–	978	0.06	960	0.07	1031	6.31	γHCCC(74)	νCC(39)	τNCCC(41)
–	–	–	972	0.04	957	0.07	1011	19.72	γHCCC(76)	δCCC(10)	δCCC(10)
–	940	–	955	0.07	938	0.06	1009	0.83	τCCCC(16)	γHCCC(63)	νCC(13)
–	–	–	941	1.62	933	2.59	1008	0.07	δCCC(10)	τCCCC(17)	γHCC(12)
934	–	–	939	0.46	932	0.92	998	0.51	γHCCC(79)	γHCCC(17)	δCCC(17)

–	–	–	932	1.09	901	1.58	990	0.09	γHCCC(71)	γHCCC(10)	γHCC(15)
910	892	–	914	0.03	894	2.18	983	0.07	γHCCC(78)	γHCCC(44)	δCCC(14)
–	–	–	898	0.10	876	0.86	978	0.14	δCCC(15)	γHCCC(46)	δCCC(11)
–	871	–	887	0.43	872	1.40	948	1.78	γHCCC(45)	γHCCC(58)	δCCC(14)
880	–	–	882	3.91	803	0.08	945	0.10	γHCCC(62)	τCCCC(15)	νNN(58)
–	–	945	873	7.65	791	12.80	945	1.65	τCCCC(13)	δCCC(21)	δOCN(10)
–	–	–	850	0.03	787	0.00	942	0.80	γHCCC(59)	γHCCC(62)	δCCC(17)
–	776	928	830	7.32	774	1.24	927	7.19	σCCC(10)	γHCCC(66)	γHCCC(19)
–	–	910	820	2.07	773	0.25	906	0.26	δCCC(28)	τCCCC(12)	γHCCC(29)
775	758	–	776	3.46	759	1.04	891	0.29	γHCCC(57)	γNCC(10)	γHCCC(22)
–	742	868	773	0.78	741	3.86	869	8.49	τOCOC(11)	γHCCC(67)	γHCCC(44)
–	–	–	766	1.12	739	0.76	853	0.68	γHCCC(87)	τCCCC(11)	γHCCN(38)
–	713	–	749	0.13	715	1.62	845	10.38	γHCCC(10)	γHCCC(79)	γHCCC(18)
710	–	839	721	1.12	713	0.11	836	22.27	γHCCC(72)	γHCCC(54)	γHCCC(44)
–	–	–	705	4.84	669	4.65	832	10.48	γHCCC(20)	δCCC(29)	γHCCC(14)
–	–	–	699	1.86	656	0.73	805	2.88	νBrC(24)	δCCC(21)	γHCCC(12)
–	–	–	660	0.35	648	2.78	776	3.88	τCCNC(18)	τCCCC(25)	δCCC(11)
–	645	–	651	1.27	646	0.14	773	9.08	δCCC(17)	τOCOC(38)	τOCNC(14)
–	–	754	644	4.11	636	3.47	751	0.41	τCCCC(43)	δCCC(11)	γHCCC(64)
631	–	–	630	0.43	629	0.27	740	12.50	νBrC(26)	δCCC(20)	δCCC(18)
–	–	–	614	0.81	618	11.26	724	5.99	δCCC(29)	δCCC(18)	γHCCC(25)
–	608	712	596	2.10	608	7.43	710	7.82	τCCCC(11)	γHCCC(58)	τHCNN(29)
592	–	–	591	6.62	605	7.21	702	12.92	γCCN(49)	δCCC(23)	δCCC(17)
–	561	–	556	14.51	565	6.80	661	1.43	δCCC(42)	γCCN(10)	δCCC(18)
552	–	652	554	7.82	546	4.71	650	1.77	γOCO(10)	δCCC(54)	γNNC(13)
–	–	628	518	2.11	511	0.71	637	2.78	δCCC(18)	τCCCC(10)	νBrC(36)
–	498	–	498	0.31	499	0.98	629	0.23	δCCC(69)	νBrC(24)	τCCCC(10)
–	–	610	468	3.32	469	2.93	608	1.93	δCCC(38)	δCCC(63)	τCCCC(18)
–	443	–	456	0.20	441	0.02	599	4.28	τCCCC(16)	τHOCC(61)	τCCCC(14)
–	432	–	449	0.49	430	0.12	594	0.56	τCCCC(13)	τCCCN(245)	τCCNC(17)
432	–	541	434	1.02	420	1.35	546	0.84	τHOCC(79)	τCCNC(12)	τHNNC(36)
–	–	–	416	0.12	400	0.61	540	1.62	τCCCC(53)	τCCCN(14)	τCCCC(15)
–	–	–	377	0.17	378	0.02	532	11.14	τNCCC(20)	τNCCC(17)	τCCCC(14)
–	–	498	352	0.12	362	0.67	499	5.41	γCNC(11)	τCCCN(23)	τCCCC(29)
–	–	–	324	0.11	347	0.09	494	1.52	τCCNC(39)	τCCCC(11)	δCCC(10)
–	–	448	297	0.22	334	1.32	448	0.57	τCCCC(10)	νNC(12)	δCCC(15)
–	–	–	269	0.03	311	0.00	447	1.12	τCCNC(16)	δCCC(11)	τCCCC(19)
–	–	–	257	0.03	290	0.14	426	4.20	γCNC(11)	τCCCN(12)	τCCCC(11)
–	–	–	230	0.12	241	0.00	413	0.83	δCCC(12)	τCCCN(11)	δCCC(17)
–	–	410	210	0.03	233	0.04	411	0.31	τCCCN(16)	δCCC(63)	τCCCN(13)
–	–	–	188	0.02	227	0.16	380	3.04	τCCCN(24)	τCCCC(12)	τCCCN(10)
–	–	–	183	0.12	218	0.02	351	0.14	τCCCN(53)	τCCNC(18)	τNNCC(23)
–	–	–	151	0.16	200	0.22	331	0.03	γBrCC(22)	γCCO(31)	τNCCC(25)
–	–	–	119	0.04	149	0.26	325	0.37	τCCNC(12)	γBrCC(21)	τCCNC(13)
–	–	–	115	0.13	141	0.06	310	0.03	γBrCC(32)	δNCC(20)	τCNCC(17)
–	–	–	88	0.02	136	0.19	283	0.46	τCCCO(51)	τCCNC(40)	γNCC(18)
–	–	–	60	0.03	104	0.13	247	0.16	τCCCN(68)	δCCC(11)	δCCN(8)
–	–	–	58	0.06	95	0.10	227	0.27	τNCCC(14)	δCCC(32)	δNCC(27)
–	–	–	46	0.08	70	0.38	211	0.01	τCCCC(17)	δCCC(12)	δCCN(13)
–	–	–	40	0.07	55	0.00	206	0.09	τCCCC(13)	τCNCC(35)	γBrCC(10)
–	–	–	35	0.20	51	0.03	172	0.76	τCCCC(72)	τCCCN(17)	δCCN(14)
–	–	–	26	0.06	45	0.04	165	0.41	τCNCC(78)	τCCCN(53)	τBrCCC(15)
–	–	–	–	–	36	0.16	157	0.09	–	δCCC(54)	γBrCC(13)
–	–	–	–	–	22	0.06	108	0.16	–	τOCCC(80)	δCCC(20)
–	–	–	–	–	11	0.00	85	0.05	–	δCCC(59)	τNCCC(13)
–	–	–	–	–	–	–	82	0.05	–	–	δCNC(12)
–	–	–	–	–	–	–	75	0.16	–	–	δCNN(13)
–	–	–	–	–	–	–	52	0.14	–	–	τCNNC(20)
–	–	–	–	–	–	–	48	1.09	–	–	γNCC(18)
–	–	–	–	–	–	–	34	0.31	–	–	τCCCN(63)
–	–	–	–	–	–	–	23	0.11	–	–	δCNC(22)
–	–	–	–	–	–	–	8	0.55	–	–	τCCNN(31)

as sensitizers. The photosensitization features have characterized these dye compounds as possible candidates for the manufacture of dye-sensitized solar cells (DSSCs). The contributions of phenyl-carbazole act as a donor unit and serve as an acceptor of acrylic acid, cyanoacrylic acid and cyanoaceto-hydrazide. The incorporation of an acceptor improves ICT and therefore J_{SC} due to its enhanced drawing capability. The results of FMO analysis of BPA, BPCA and BPCH suggested the electron transfer efficiency of the D-π-A system. The results showed that phenyl-carbazole organic sensitizers have been showing promise to further improves the conversion efficiency of DSSCs due to the original and flexible molecular design.

ACKNOWLEDGEMENTS

The authors are grateful to the Central Laboratory of the Vellalar Women's College for providing the spectral analysis.

CONFLICT OF INTEREST

The authors declare that there is no conflict of interests regarding the publication of this article.

REFERENCES

1. R. Su, L. Lyu, M.R. Elmorsy and A. El-Shafei, *Sol. Energy*, **194**, 400 (2019); https://doi.org/10.1016/j.solener.2019.10.061
2. P. Naik, R. Su, M.R. Elmorsy, A. El-Shafei and A.V. Adhikari, *Dyes Pigments*, **149**, 177 (2018); https://doi.org/10.1016/j.dyepig.2017.09.068
3. S. Namuangruk, R. Fukuda, M. Ehara, J. Meeprasert, T. Khanasa, S. Morada, T. Kaewin, S. Jungsuttiwong, T. Sudyoadsuk and V. Promarak, *J. Phys. Chem. C*, **116**, 25653 (2012); https://doi.org/10.1021/jp304489t
4. J. Yang, P. Ganesan, J. Teuscher, T. Moehl, Y.J. Kim, C. Yi, P. Comte, K. Pei, T.W. Holcombe, M.K. Nazeeruddin, J. Hua, S.M. Zakeeruddin, H. Tian and M. Gratzel, *J. Am. Chem. Soc.*, **136**, 5722 (2014); https://doi.org/10.1021/ja500280r
5. S.E. Koops, B.C. O'Regan, P.R.F. Barnes and J.R. Durrant, *J. Am. Chem. Soc.*, **131**, 4808 (2009); https://doi.org/10.1021/ja8091278
6. N.S. Lewis and D.G. Nocera, *Proc. Natl. Acad. Sci. USA*, **103**, 15729 (2006); https://doi.org/10.1073/pnas.0603395103
7. S. Mathew, A. Yella, P. Gao, R. Humphry-Baker, B.F.E. Curchod, N. Ashari-Astani, I. Tavernelli, U. Rothlisberger, M.K. Nazeeruddin and M. Grätzel, *Nat. Chem.*, **6**, 242 (2014); https://doi.org/10.1038/nchem.1861
8. D. Devadiga, M. Selvakumar, P. Shetty, M.S. Santosh, R.S. Chandrabose and S. Karazhanov, *Int. J. Energy Res*., **45**, 6584 (2021); https://doi.org/10.1002/er.6348
9. R.J. Sippola, A. Hadipour, T. Kastinen, P. Vivo, T. I. Hukka, T. Aernouts and J.P. Heiskanen, *Dyes Pigments*, **150**, 79 (2018); https://doi.org/10.1016/j.dyepig.2017.11.014
10. P. Thongkasee, A. Thangthong, N. Janthasing, T. Sudyoadsuk, S. Namuangruk, T. Keawin, S. Jungsuttiwong and V. Promarak, *ACS Appl. Mater. Interfaces*, **6**, 8212 (2014); https://doi.org/10.1021/am500947k
11. A. Venkateswararao, K.R.J. Thomas, C.P. Lee, C.T. Li and C. Ho, *ACS Appl. Mater. Interfaces*, **6**, 2528 (2014); https://doi.org/10.1021/am404948w
12. R. Ketavath, K.P.K. Naik, S.G. Ghugal, N.K. Katturi, T. Swetha, V.R. Soma and B. Murali, *J. Mater. Chem.*, **8**, 16188 (2020); https://doi.org/10.1039/D0TC03866K
13. M.J. Frisch, G.W. Trucks, H.B. Schlegel, G.E. Scuseria, M.A. Robb, J.R. Cheeseman, G. Scalmani, V. Barone, B. Mennucci, G.A. Petersson, H. Nakatsuji, M. Caricato, X. Li, H.P. Hratchian, A.F. Izmaylov, J. Bloino, G. Zheng, J.L. Sonnenberg, M. Hada, M. Ehara, K. Toyota, R. Fukuda, J. Hasegawa, M. Ishida, T. Nakajima, Y. Honda, O. Kitao, H. Nakai, T. Vreven, J.A. Montgomery Jr., J.E. Peralta, F. Ogliaro, M. Bearpark, J.J. Heyd, E. Brothers, K.N. Kudin, V.N. Staroverov, T. Keith, R. Kobayashi, J. Normand, K. Raghavachari, A. Rendell, J.C. Burant, S.S. Iyengar, J. Tomasi, M. Cossi, N. Rega, J.M. Millam, M. Klene, J. E. Knox, J.B. Cross, V. Bakken, C. Adamo, J. Jaramillo, R. Gomperts, R.E. Stratmann, O. Yazyev, A.J. Austin, R. Cammi, C. Pomelli, J.W. Ochterski, R.L. Martin, K. Morokuma, V.G. Zakrzewski, G.A. Voth, P. Salvador, J.J. Dannenberg, S. Dapprich, A.D. Daniels, O. Farkas, J.B. Foresman, J.V. Ortiz, J. Cioslowski and D.J. Fox, GAUSSIAN 09, revision B.01.; Gaussian Inc.: Wallingford, CT (2010).
14. M. Muthukkumar, T. Bhuvaneswari, G. Venkatesh, C. Kamal, P. Vennila, S. Armakovic, S.J. Armakovic, Y. Sheena Mary and C. Yohannan Panicker, *J. Mol. Liq.*, **272**, 481 (2018); https://doi.org/10.1016/j.molliq.2018.09.123
15. R.G. Pearson, Chemical Hardness: Applications from Molecules to Solids, Wiley: Hoboken (1997).
16. R.S. Mulliken, *J. Chem. Phys.*, **3**, 573 (1935); https://doi.org/10.1063/1.1749731
17. G. Venkatesh, M. Govindaraju, C. Kamal, P. Vennila and S. Kaya, *RSC Adv.*, **7**, 1401 (2017); https://doi.org/10.1039/C6RA25535C
18. T. Koopmans, *Physica*, **1**, 104 (1934); https://doi.org/10.1016/S0031-8914(34)90011-2
19. S. TamilSelvan, A. Prakasam, G. Venkatesh, C. Kamal, Y.S. Mary, S.P. Banu, P. Vennila and Y.S. Mary, *Z. Phys. Chem*., (2020). https://doi.org/10.1515/zpch-2020-1732
20. Y.F. Liu, J. Guan, D. Hu, L. Du, H. Sun, J. Gao, J. Zhao and Z. Lan, *J. Phys. Chem. C*, **119**, 8417 (2015); https://doi.org/10.1021/jp507746p
21. F. De Angelis, S. Fantacci and A. Selloni, *Nanotechnology*, **19**, 424002 (2008); https://doi.org/10.1088/0957-4484/19/42/424002
22. M. Pastore, S. Fantacci and F. De Angelis, *J. Phys. Chem. C*, **117**, 3685 (2013); https://doi.org/10.1021/jp3095227
23. X. Zarate, S. Schott-Verdugo, A. Rodriguez-Serrano and E. Schott, *J. Phys. Chem. A*, **120**, 1613 (2016); https://doi.org/10.1021/acs.jpca.5b12215
24. K. Takimiya, I. Osaka and M. Nakano, *Chem. Mater.*, **26**, 587 (2014); https://doi.org/10.1021/cm4021063
25. A. Kurowska, P. Zassowski, A.S. Kostyuchenko, T.Y. Zheleznova, K.V. Andryukhova, A.S. Fisyuk, A. Pron and W. Domagala, *Phys. Chem. Chem. Phys.*, **19**, 30261 (2017); https://doi.org/10.1039/C7CP05155G
26. P. Vennila, M. Govindaraju, G. Venkatesh, C. Kamal, Y.S. Mary, C.Y. Panicker, S. Kaya, S. Armakovic and S.J. Armakovic, *J. Mol. Struct.*, **1151**, 245 (2018); https://doi.org/10.1016/j.molstruc.2017.09.049
27. G. Venkatesh, C. Kamal, P. Vennila, M. Govindaraju, Y.S. Mary, S. Armakovic, S.J. Armakovic, S. Kaya and C.Y. Panicker, *J. Mol. Struct.*, **1171**, 253 (2018); https://doi.org/10.1016/j.molstruc.2018.06.001
28. M. Muthukkumar, C. Kamal, G. Venkatesh, C. Kaya, S. Kaya, I.V.M.V. Enoch, P. Vennila and R. Rajavel, *J. Mol. Struct.*, **1147**, 502 (2017); https://doi.org/10.1016/j.molstruc.2017.06.132
29. A.M. John, R. Thomas, S.P. Balakrishnan, N. Al-Zaqri, A. Alsalme and I. Warad, *Z. Phys. Chem*., (2020); https://doi.org/10.1515/zpch-2020-1722
30. N.B. Colthup, L.H. Daly and S.H. Wiberly, Introduction to Infrared and Raman Spectroscopy, Academic Press: New York, pp. 1155-1156 (1990).
31. G. Socrates, IR Characteristic Group Frequencies, John Wiley & Sons: New York (1981).
32. P. Vennila, M. Govindaraju, G. Venkatesh and C. Kamal, *J. Mol. Struct.*, **1111**, 151 (2016); https://doi.org/10.1016/j.molstruc.2016.01.068